Visual-guided Robotic Object Grasping using Dual Neural Network Controllers

Fang, Wubing; Chao, Fei; Lin, Chih-Min; Zhou, Dajun; Yang, Longzhi ; Chang, Xiang; Shen, Qiang; Shang, Changjing

Published in:
IEEE Transactions on Industrial Informatics

DOI:
10.1109/TII.2020.2995142

Publication date:
2020

Citation for published version (APA):
Fang, W., Chao, F., Lin, C-M., Zhou, D., Yang, L., Chang, X., Shen, Q., & Shang, C. (Accepted/In press). Visual-guided Robotic Object Grasping using Dual Neural Network Controllers. *IEEE Transactions on Industrial Informatics*. https://doi.org/10.1109/TII.2020.2995142

This article has been accepted for publication in a future issue of this journal, but has not been fully edited. Content may change prior to final publication. Citation information: DOI 10.1109/TII.2020.2995142, IEEE Transactions on Industrial Informatics

Visual-guided Robotic Object Grasping using Dual Neural Network Controllers

Wubing Fang, Fei Chao, *Member, IEEE,* Chih-Min Lin, *Fellow, IEEE,* Dajun Zhou, Longzhi Yang, *Senior Member, IEEE,* Xiang Chang, Qiang Shen, and Changjing Shang,

***Abstract*—It has been a challenging task for a robotic arm to accurately reach and grasp objects, and much research attention has been attracted. This paper proposes a robotic hand-eye coordination system by simulating the human behavior pattern to achieve a fast and robust reaching ability. This is achieved by two neural-network-based controllers, including a rough reaching movement controller implemented by a pre-trained Radial Basis Function (RBF) for rough reaching movements, and a correction movement controller built from a specifically designed Brain Emotional Nesting Network (BENN) for smooth correction movements. In particular, the proposed BENN is designed with high nonlinear mapping ability, with its adaptive laws derived from the Lyapunov stability theorem; from this, the robust tracking performance and accordingly the stability of the proposed control system are guaranteed by the utilisation of the H^∞ control approach. The proposed BENN is validated and evaluated by a chaos synchronisation simulation, and the overall control system by object grasping tasks through a physical robotic arm in a real-world environment. The experimental results demonstrate the superiority of the proposed control system in reference to those with single neural networks.**

***Index Terms*—Robotic hand-eye coordination, neural network-based controller, robotic reaching movement**

I. Introduction

The key for a successful vision-based robotic manipulator system with reaching ability is effective hand-eye coordination [1], which uses the information obtained from vision sensors to guide robotic manipulators to reach and manipulate the target objects [2]–[4]. Hand-eye coordination combines the technologies in computer vision and robotics to enhance robotic sensory-motor ability [5]–[7], which plays an important role in industrial assembly robots [8]–[10], mobile exploration robots [11], and robots for education, medical, military, etc [12]. Traditional hand-eye coordination works based on the accurate kinematic calibrations between the robotic hand and vision system, which are usually designed by human engineers [13]. However, it is getting increasingly more difficult to handle real-world applications using such hand-crafted approaches, leading to the requirement of adaptability for intelligent robots [14]. Therefore, various neural networks and artificial infant developmental approaches have been developed.

Challenges remain to be solved for the adaptation of infant development patterns to visual-guided robotic reaching. Vision-guided manipulators usually move inaccurately and react slowly, as the mappings between robotic vision and manipulator is highly non-linear [15], [16], which forms one of the main challenges. Visual-guided robotic reaching is usually implemented using neural network-based approaches due to its non-linear mapping ability [17]–[19]. For instance, a hand-eye coordination system based on the three Radial Basis Functions is reported in [20]; and a large convolutional network has been developed to observe the spatial relationship between robotic arm and target [17]. However, those systems either presents a long leeway for adjustments and training, or low accuracy of the robot actions.

Human-like behavioral patterns have been used for hand-eye coordination, in an effort to reduce the complexity of robot learning and thus ease the first challenge, but they are often lack of a solid theoretical foundation and its analysis for stability [15], [20]. Of course, an unstable system often leads to inaccurate movements and poor performance for grasping tasks. If a robotic arm touches its target without accurate movements, certain unexpected damages can be expected to both the robotic arm and the target. Therefore, more efforts is required to guarantee the stability of robotic reaching system with the adaptation of human behavior patterns.

This paper proposes a robotic hand-eye coordination control system by artificially implementing human behavior patterns for robotic reaching movements. In the human infant's reaching movement, once a target object is detected, the infant can perform only a rough reaching movement towards the object in its early stage, but this activity is constantly improved and most babies can accurately reach objects in 31 weeks [21]. Inspired by this, the artificial reaching ability is established in two stages: (1) a rough reaching movement guided by vision, and (2) a smooth correction movement guided by inverse kinematics. These two stages are realised by dual neural-network-based controllers, with the first one driving the robotic arm to generate a wide range of reaching movements, whilst the second one enabling the robotic arm to perform correction movement for accurate grasp operations. Both controllers take the visual-spatial coordinates provided by a stereo vision system as network inputs.

W. Fang and F. Chao are with the Department of Artificial Intelligence, School of Informatics, Xiamen University, China (e-mail: fchao@xmu.edu.cn). C.-M. Lin is with the Department of Electrical Engineering, Yuan Ze University, Taiwan. (e-mail: cml@saturn.yzu.edu.tw). D. Zhou is with the Huawei Technologies Co Ltd., Shenzhen, China (e-mail: 860122112@qq.com). L. Yang is with the Department of Computer and Information Sciences, Northumbria University, UK (e-mail: longzhi.yang@northumbria.ac.uk). F. Chao, C. Xiang, C. Shang and Q. Shen are with the Department of Computer Science, Institute of Mathematics, Physics and Computer Science, Aberystwyth University, SY23 3DB, UK (e-mail: {fec10,xic9,cns,qqs}@aber.ac.uk). Corresponding author: Fei Chao.

This work was supported by the Fundamental Research Funds for the Central Universities (No. 20720190142), the National Natural Science Foundation of China (No. 61673322, 61673326, and 91746103), and the European Union's Horizon 2020 research and innovation programme under the Marie Sklodowska-Curie grant agreement No. 663830.

This article has been accepted for publication in a future issue of this journal, but has not been fully edited. Content may change prior to final publication. Citation information: DOI 10.1109/TII.2020.2995142, IEEE Transactions on Industrial Informatics

The proposed hand-eye coordination control system was evaluated using target-reaching experiments, whilst the correction movement controller was additionally verified by a chaos synchronization simulation. The experimental results show that the proposed controller can achieve a higher success rate and better control performance, which effectively alleviating the aforementioned challenges faced in the field. The contributions of this paper are: (1) establishing a robotic hand-eye coordination control system implemented in two stages; (2) proving the stability and convergence of the proposed system using the Lyapunov stability theorem, which is guaranteed by the network learning rules.

The remainder of this paper is organized as follows: Section II introduces the development procedure of infant reaching movement and the platform of the hand-eye coordination system established. Section III describes the implementation details of the proposed robotic hand-eye coordination control system. Section IV shows the experimental results. Section V concludes the paper and points out important future work.

II. Background and Platform

The developmental procedures of infant reaching movement have been recently well studied by developmental psychologists [21]. In the first two months after birth, infants can only generate brief extension movements attempting to touch nearby objects by their hands [22]; and these extension movements cannot successfully touch targets every time. However, after 31 weeks, infants are able to use the distance between hands and objects, measured through eyes, to adjust the position and orientation of hand to reach targets [23]. In other words, infants gradually develop error correction movements to achieve accurate object reaching ability. Such discovered development sequences are very informative for artificial hand-eye coordination development.

Inspired by the developmental procedures of infants reaching ability, a typical robotic hand-eye coordination system platform was also used in this paper, as shown in Fig. 1. The platform is comprised of a depth vision sensor and a robotic arm. In particular, the depth vision sensor is used to acquire the positions of the robotic arm and a target in the workspace; while the robotic arm is responsible for performing the desired reaching movements and the grasp actions. The mobility of the platform in this work is implemented for capturing targets beyond the reaching area of the robotic arm.

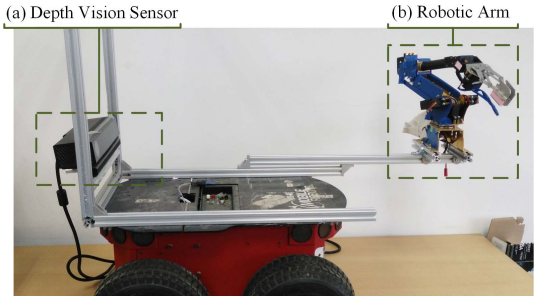

Fig. 1. Platform of the robotic hand-eye coordination system.

The robotic vision system is mainly formed by a depth vision sensor (Kinect) with the support of an image processing module, which calculates the visual-spatial coordinates of the robotic arm and the target to guide the movement of the robotic arm. The depth vision sensor captures an RGB image of the workspace, including the "Shoulder", "Wrist", and "Grip" joints of the robotic arm and the target. Then, the target is recognized from the image by employing the minimum peripheral circle program in OpenCV, which also helps determine the coordinates of the joints. From this, the 3-dimensional coordinates of the joints and target in the stereo space are calculated using the Kinect SDK.

The robotic arm is a five-degree-of-freedom parallelogram robotic arm with six servo motors, which can be expressed by the following second-order equation [24]–[26]:

$$B(q)\ddot{q} + C(q,\dot{q})\dot{q} + g(q) + \tau_d = \tau, \tag{1}$$

where $q = (\theta_1, \theta_2, \ldots, \theta_m)^T$ denotes the joint angle vector of the robotic arm, $\dot{q}$ and $\ddot{q}$ are respectively the corresponding angular velocity vector and angular acceleration vector, $B(q)$ represents the inertia matrix, $C(q,\dot{q})$ indicates the Coriolis/Centripetal matrix, $g(q)$ expresses the gravity vector, $g = 9.8m/s$ is gravity acceleration, τ_d represents external disturbance, and $\tau = (S_1, S_2, \ldots, S_m)$ is the output torques of servo at each joint. For the illustrated robotic arm, m is set to 6.

The parameters of the accurate system model are unknown; however, the neural network can approximate a corresponding nominal model of the platform, which is defined as:

$$B_n(q)\ddot{q} + C_n(q,\dot{q})\dot{q} + g(q) = \tau, \tag{2}$$

where $B_n(q)$ and $C_n(q,\dot{q})$ are the nominal functions of $B(q)$ and $C(q,\dot{q})$, respectively. Then Eq. (1) can be re-expressed as:

$$B_n(q)\ddot{q} + C_n(q,\dot{q})\dot{q} + g(q) + l(\ddot{q},\dot{q},q) = \tau, \tag{3}$$

where $l(\ddot{q},\dot{q},q) = \Delta B_n(q)\ddot{q} + \Delta C_n(q,\dot{q})\dot{q} + \tau_d$ denotes the lumped disturbances and uncertainties.

III. Robotic Hand-eye Coordination System

Inspired by the infant developmental procedure of reaching and grasping ability, the robotic reaching movement is implemented by dual network-based controllers in two training stages. Stage one implements a rough reaching process, by which the robotic arm can roughly reach targets by large range movements. This process does not require well-developed nonlinear mapping abilities; therefore, a pre-trained Radial Basis Function network-based controller is established to map the manipulator moments to the visual inputs. Stage two realises small refinement correction movements, to enable a smooth and accurate reaching movements. The correction movements can only be implemented by a controller with higher nonlinear mapping abilities, so as to deal with the highly non-linear mapping between angular tracking errors for the joints of the manipulator and the states of the joint motor. Studies show that a better nonlinear mapping ability can be achieved if an additional network is embedded in the emotional networks [27].

This article has been accepted for publication in a future issue of this journal, but has not been fully edited. Content may change prior to final publication. Citation information: DOI 10.1109/TII.2020.2995142, IEEE Transactions on Industrial Informatics

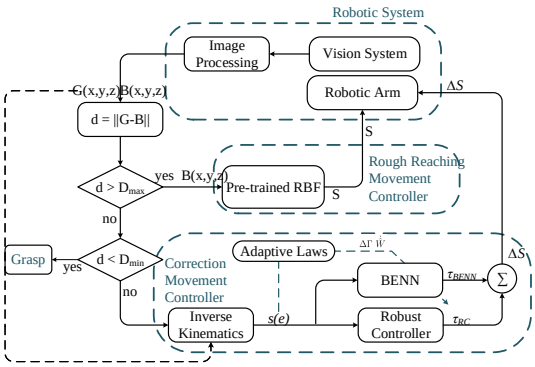

Fig. 2. The proposed robotic hand-eye coordination system with dual neural-network-based controllers.

Fig. 3. Input and output of image processing. (a) Detections of Robotic shoulder; (b) robotic wrist and gripper; and (c) target.

Therefore, a new type of Brain Emotional Nesting Network (BENN) is proposed here for the correction movements.

The framework of the proposed control system is shown in Fig. 2, which consists of a robotic system module, a rough reaching movement controller, and a correction movement controller. First, the positions of the robotic gripper, $G(x, y, z)$, and target, $B(x, y, z)$, are acquired by processing the information acquired from the vision system. The position error between the gripper and the target is then calculated using the Euclidean distance.

Note that the distance between the griper and the object may change over time due to gripper movement errors or environment changes, therefore, the two controllers and thus the two stages of training may be triggered at any time in any order when performing an object reaching task. Two thresholds, $D_{\max}$ and $D_{\min}$, are employed in this work to distinguish the application of the two controllers: if $d > D_{\max}$, the robotic arm is controlled by the rough reaching movement controller with a pre-trained RBF network to perform rough reaching actions; if $D_{\min} < d < D_{\max}$, the correction movement controller with the proposed BENN neural network is used to control the robotic arm as the robotic arm has moved to a position that is close to the target and must perform a smooth correction movements to complete the grasping; otherwise, the robotic arm performs a grasping action. The two controllers are detailed in the rest of this section below.

A. Vision System

The image processing function in the vision system is designed to obtain the position coordinates of the target and the robot's Shoulder, Wrist, and Grip in the workspace, which in turn are used to calculate the inputs of the robotic control system. The left column of Fig. 3 demonstrates some captured RGB images from the Kinect device. To simplify the image processing task, the Shoulder was marked in green, and Wrist and Grip are marked in pink; an orange ball was used as the capturing target. The RGB color ranges of the Shoulder mark (i.e., green), the Wrist and Grip (i.e., pink), and the target Ball (i.e., orange) were set to $(50-78,\ 70-150,\ 100-230)$, $(160-180,\ 57-140,\ 140-255)$, and $(20-35, 130-240, 0-255)$, respectively. The Wrist and Grip were distinguished by the movement region size, that Grip owns a larger size whilst the Wrist owns a smaller one. With the defined color ranges, the joints and the target can be detected as clusters in the binarization images (as shown in the right column of Fig. 3) by using the RGB color ranges. Then, the position coordinates of each cluster can be obtained accurately in the stereo space using the Kinect SDK.

B. Rough Reaching Movement Controller

The rough reaching movement controller implemented by a RBF neural network is triggered to drive the robotic arm to move when the distance between the gripper and the object is bigger than the pre-defined threshold $D_{\max}$. The input of the RBF-based controller is the position of the target, $B(x, y, z)$, and the output is the servo speed, $(S_1, S_2, S_3, S_4, S_5, S_6)$, of each robotic arm joint, based on the position of the griper. The pose of the gripper and target can be calculated based on the robotic arm's shoulder, $Shoulder(x, y, z)$, which is defined as the origin of the base coordinate system.

The RBF used in this work consists of 55 hidden nodes, which was determined empirically. The weights of these nodes are denoted as ν_j, $j = 0, 1, 2, \ldots, 55$, and the outputs of the RBF are denoted as $R(\nu)$. Define $h_\nu^{(i)} = (x_b, y_b, z_b, R(\nu)_1, R(\nu)_2, R(\nu)_3, R(\nu)_4, R(\nu)_5, R(\nu)_6)$; the cost function can then be defined as $J(\nu) = \frac{1}{2}\sum_{i=1}^{55}(h_\nu^{(i)} - t^{(i)})^2$. The stochastic gradient descent algorithm is employed to train the RBF network, which can be expressed as $\nu_j := \nu_j - \alpha_{RBF}\frac{\partial}{\partial \nu_j}J(\nu)$, where α_{RBF} is the learning rate.

In order to train the RBF, a motor-babbling inspired movement pattern is developed to generate the training data. First, the target position, $B(x_b, y_b, z_b)$, is substituted by the position of the gripper, $G(x_g, y_g, z_g)$, denoted as (x_s, y_s, z_s). Then, the servo is randomly driven to simulate the motor-babbling movements occurred in an infants development. Thus, for the i-th movement, a sample of training data, $t^{(i)} = (x_s, y_s, z_s, S_1, S_2, S_3, S_4, S_5, S_6)$, is obtained, representing the servo speed of each robotic manipulate joint. Based on some empirical study, a training data set based on 3,000 movements usually leads to good acceptable results, with 2,000 instances for training and the rest for testing.

This article has been accepted for publication in a future issue of this journal, but has not been fully edited. Content may change prior to final publication. Citation information: DOI 10.1109/TII.2020.2995142, IEEE Transactions on Industrial Informatics

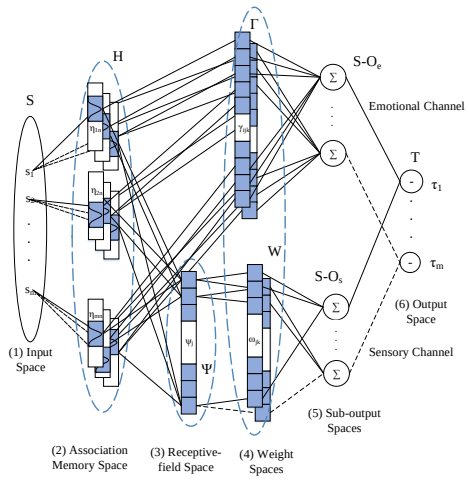

Fig. 4. The architecture of proposed BENN.

C. Correction Movement Controller

The robotic arm generates correction movements when the distance between the griper and the object is between the pre-defined thresholds, $D_{\min}$ and $D_{\max}$, so that the robotic arm can smoothly and accurately grasp the target. The joint angle vector, $q_d = (\theta_1^d, \theta_2^d, \ldots, \theta_m^d)^T$, needs to be calculated by using inverse kinematics. The inverse kinematic calculations can convert the errors between the target and gripper to the relative values of the robot's joints.

The correction movement controller is comprised of a BENN and a robust controller. The input of the BENN-based controller is the combined error $s(\underline{e})$, which is specified as:

$$s(\underline{e}) = [I, K] \begin{bmatrix} \dot{e} \\ e \\ \int_0^T e(t)dt \end{bmatrix}, \tag{4}$$

where $\underline{e} = [\dot{e}, e, \int_0^T e(t)dt]^T$, $e = q_d - q$, whilst $q = (\theta_1, \theta_2, \ldots, \theta_m)^T$ is the current joint angle vector. In addition, K is an error matrix, which is defined as:

$$K = \begin{bmatrix} \rho_{11} & & \rho_{21} & & \\ & \ddots & & \ddots & \\ & & \rho_{1m} & & \rho_{2m} \end{bmatrix} \in \Re^{m \times 2m}, \tag{5}$$

where ρ_{ij} is the combination coefficient, for $i = 1, 2, j = 1, 2, \ldots, m$. For this robotic arm, m is set to 6.

The output of the BENN-based controller is $\tau_{BENN} = (\Delta S_1, \Delta S_2, \ldots, \Delta S_m)$, where ΔS_m denotes the increment of the mth joint servo. It is guaranteed that the entire system (both rough reaching movement and correction movement controllers) is stable once the robotic arm reaches a wide range of the target space (i.e., in the correction movement stage). The structure and adaptive laws of the proposed BENN are detailed below.

1) The proposed BENN: The structure of proposed BENN neural network is shown in Fig. 4, which consists of (1) the input space, $S \in \Re^m$, (2) the association memory space, $H \in \Re^{mn}$, (3) the receptive field space, $\Psi \in \Re^n$, (4) the weight spaces, $\Gamma \in \Re^{mn \times m}$ and $W \in \Re^{n \times m}$, (5) the sub-output spaces, $S - O_e \in \Re^m$ and $S - O_s \in \Re^m$, and (6) the output space, $T \in \Re^m$. Note that the network is divided into two channels from the association memory space. One channel mimics the emotional channel in brain emotional learning, which consists of a weight space Γ, whilst the other channel simulates the function of the sensory channel in brain emotional learning, comprising of the receptive field space Ψ and the weight space W. The final output of the network, $\tau = o_e - o_s$, is the difference of the outputs of the two channels, where the output of the emotional channel is defined as $o_e = \Gamma^T \cdot H$, and the output of the sensory channel is defined as $o_s = W^T \cdot \Psi$.

2) Adaptive laws of BENN: Taking the derivative of (4) and applying (3), yields:

$$\dot{s}(\underline{e}) = \ddot{q}_d - B_n^{-1}[\tau - C_n\dot{q} - g - l] + K \begin{bmatrix} \dot{e} \\ e \end{bmatrix}. \tag{6}$$

This means the control system will be stable if $s(\underline{e})\dot{s}(\underline{e}) \leq -\sum_{i=1}^m \beta_i |s_i|$, for $\beta_i > 0$, $i = 1, 2, \ldots, m$. In addition, an ideal controller τ_{IDEAL} for correction movement can be defined as:

$$\begin{aligned} \tau_{IDEAL} =& B_n\ddot{q}_d + C_n\dot{q} + g + l \\ &+ B_n K \begin{bmatrix} \dot{e} \\ e \end{bmatrix} + B_n \cdot \beta \cdot sgn(s(\underline{e})), \end{aligned} \tag{7}$$

where $sgn(\cdot)$ is a symbolic function. However, the ideal controller τ_{IDEAL} is not available. Therefore, the ideal controller is approximated by the proposed correction movement controller, consisting of a BENN-based controller and a robust controller.

The adaptive laws of the sensory channel in the proposed BENN are derived from the Lyapunov stability theorem, whilst those of the emotional channel are given by the brain emotional learning. Therefore, residual approximation errors $\tilde{\Gamma}$ and $\tilde{W}$ exist between the ideal weights Γ^*, W^* and the estimated weights $\hat{\Gamma}$, $\hat{W}$. In addition, an attenuation of the approximation error ε presents between the ideal controller output τ_{IDEAL} and the output of BENN τ_{BENN}^*. The robust controller is used to compensate for $\tilde{\Gamma}$ and ε. The robust tracking performance of the controller is guaranteed base on the H^∞ control approach [28].

Subtracting (7) from (6), yields:

$$\dot{s}(\underline{e}) = B_n^{-1}[\tau_{IDEAL} - \tau_{controller}] - \beta \cdot sgn(s(\underline{e})), \tag{8}$$

where τ_{IDEAL} can be represented as:

$$\tau_{IDEAL} = \tau_{BENN}^* + \varepsilon = \Gamma^{*T} H - W^{*T}\Psi + \varepsilon, \tag{9}$$

and $\tau_{controller}$ can be calculated as:

$$\tau_{controller} = \tau_{BENN} + \tau_{RC} = \hat{\Gamma}^T H - \hat{W}^T\Psi + \tau_{RC}, \tag{10}$$

where $\tilde{\Gamma} = \Gamma^* - \hat{\Gamma}$, $\tilde{W} = W^* - \hat{W}$. Applying (9) and (10) to (8) leads to:

$$\begin{aligned} \dot{s}(\underline{e}) =& B_n^{-1}[\Gamma^{*T} H - W^{*T}\Psi + \varepsilon - \hat{\Gamma}^T H + \hat{W}^T\Psi \\ &- \tau_{RC}] - \beta \cdot sgn(s(\underline{e})) \\ =& B_n^{-1}[\tilde{\Gamma}^T H - \tilde{W}^T\Psi + \varepsilon - \tau_{RC}] - \beta \cdot sgn(s(\underline{e})). \end{aligned} \tag{11}$$

This article has been accepted for publication in a future issue of this journal, but has not been fully edited. Content may change prior to final publication. Citation information: DOI 10.1109/TII.2020.2995142, IEEE Transactions on Industrial Informatics

For the existence of $\tilde{\Gamma}$ and ε, predefined attenuation levels ς_1 and ς_2, corresponding to ε and $\tilde{\Gamma}$ respectively, can be applied to ensure a H^∞ tracking performance [16]:

$$\sum_{i=1}^{m}\int_0^T s_i^2(t)dt \le s^T(\underline{e}(0))B_n s(\underline{e}(0)) + tr[\tilde{W}^T(0)\alpha_W^{-1}\tilde{W}(0)] + \sum_{k=1}^{m}\varsigma_{1k}^2\int_0^T \varepsilon_k^2(t)dt + \sum_{k=1}^{m}\varsigma_{2k}^2\int_0^T \tilde{\gamma}_k^2(t)dt, \tag{12}$$

where α_W represents the positive definite learning rate matrix, $\tilde{\gamma}_{ijk}$ indicates the element in the matrix $\tilde{\Gamma}$. $\tilde{\Gamma}$ and ε are bounded, i.e., $\tilde{\Gamma} \in L_2[0,T_1]$ and $\varepsilon \in L_2[0,T_2]$ with $\forall T_1, T_2 \in [0,\infty)$. Note that $\tilde{\Gamma}$ is contained in ε, this means that $\tilde{\Gamma}$ will decay to 0 as ε decays to 0. Thus, it leads to $\varsigma_2 = 1$, whilst $\lambda = \varsigma_1$, which can be adjusted in τ_{RC}.

3) Proof of stability: RBF and BENN are two independent controllers with different mechanisms. The RBF controller performs rough reaching movements, as long as the training method of RBF can guarantee the tracking error to be bounded. Therefore, the stability of the entire system is based on the BENN based controller.

Theorem 1: The adaptive laws of the emotional channel in BENN can be described as:

$$\Delta\Gamma = \alpha_\Gamma[H \times \max(0, d-b)], \tag{13}$$

$$d = \alpha_{d1} \times q + \alpha_{d2} \times \tau_{BENN}, \tag{14}$$

where $\alpha_\Gamma, \alpha_{d1}, \alpha_{d2}$ are the learning rates, b is the output of the emotional channel, q is the input of entire network, and τ_{BENN} is the output of entire network. The update laws of the sensory channel in BENN can be designed as:

$$\dot{\tilde{W}} = -\alpha_W \Psi s^T(\underline{e}), \tag{15}$$

$$\tau_{RC} = (2R^2)^{-1}[(I+H^2)R^2 + I]s^T(\underline{e}), \tag{16}$$

where $R = diag\begin{bmatrix}\lambda_1 & \lambda_2 & \dots & \lambda_m\end{bmatrix} \in \Re^{m\times m}$ is a diagonal matrix of a robust controller to converge the proposed system with the update rules $\dot{\tilde{W}}$.

Proof: The Lyapunov function is given as:

$$L(s(\underline{e}), \tilde{W}) = \frac{1}{2}s^T(\underline{e})B_n s(\underline{e}) + \frac{1}{2}tr[\tilde{W}^T\alpha_W^{-1}\tilde{W}]. \tag{17}$$

Taking the derivative of the Lyapunov function and using Eqs. 11, 15, and 16, the following can be derived:

$$\begin{aligned}
&\dot{L}(s(\underline{e}), \tilde{W}) = s^T(\underline{e})B_n\dot{s}(\underline{e}) + tr[\tilde{W}^T\alpha_W^{-1}\dot{\tilde{W}}] \\
&= s^T(\underline{e})\tilde{\Gamma}^T H - s^T(\underline{e})\tilde{W}^T\Psi - tr[\tilde{W}^T\alpha_W^{-1}\dot{\tilde{W}}] \\
&+ s^T(\underline{e})(\varepsilon - \tau_{RC}) - s(\underline{e})^T \cdot B_n \cdot \beta \cdot sgn(s(\underline{e})) \\
&\le s^T(\underline{e})\tilde{\Gamma}^T H + s^T(\underline{e})(\varepsilon - \tau_{RC}) \\
&= -\frac{1}{2}s^T(\underline{e})s(\underline{e}) - \frac{1}{2}[\frac{s(\underline{e})}{\lambda} - \lambda\varepsilon]^T[\frac{s(\underline{e})}{\lambda} - \lambda\varepsilon] \\
&- \frac{1}{2}tr[[Hs^T(\underline{e}) - \tilde{\Gamma}]^T[Hs^T(\underline{e}) - \tilde{\Gamma}]] + \frac{1}{2}\lambda^2\varepsilon^T\varepsilon + \frac{1}{2}tr[\tilde{\Gamma}^T\tilde{\Gamma}] \\
&\le -\frac{1}{2}s^T(\underline{e})s(\underline{e}) + \frac{1}{2}\lambda^2\varepsilon^T\varepsilon + \frac{1}{2}tr[\tilde{\Gamma}^T\tilde{\Gamma}].
\end{aligned} \tag{18}$$

Integrating Eq. 18 from $t=0$ to $t=T$, yields:

$$\begin{aligned}
L(T) - L(0) \le &-\frac{1}{2}\sum_{i=1}^{m}\int_0^T s_i^2(t)dt \\
&+ \frac{1}{2}\sum_{k=1}^{m}\lambda_k^2\int_0^T \varepsilon_k^2(t)dt + \frac{1}{2}\sum_{k=1}^{m}\int_0^T \tilde{\gamma}_k^2(t)dt.
\end{aligned} \tag{19}$$

Since $L(T) > 0$, the following holds:

$$\begin{aligned}
&\frac{1}{2}\sum_{i=1}^{m}\int_0^T s_i^2(t)dt \le \\
&L(0) + \frac{1}{2}\sum_{k=1}^{m}\lambda_k^2\int_0^T \varepsilon_k^2(t)dt + \frac{1}{2}\sum_{k=1}^{m}\int_0^T \tilde{\gamma}_k^2(t)dt \\
&= \frac{1}{2}s^T(\underline{e}(0))B_n s(\underline{e}(0)) + \frac{1}{2}tr[\tilde{W}^T(0)\alpha_W^{-1}\tilde{W}(0)] \\
&+ \frac{1}{2}\sum_{k=1}^{m}\lambda_k^2\int_0^T \varepsilon_k^2(t)dt + \frac{1}{2}\sum_{k=1}^{m}\int_0^T \tilde{\gamma}_k^2(t)dt.
\end{aligned} \tag{20}$$

The equivalence between Eqs. 12 and 20 proves that the H^∞ tracking performance is achievable. ■

IV. Experimentation

A chaos synchronisation experiment was conducted first to verify whether the correction movement controller with the proposed BENN network is stable, without the utilisation of the rough reaching movement controller. Then, a hardware platform was established to evaluate the proposed robotic hand-eye coordination system in real-world experiments. From this, a comparative study was conducted to analyze the effects of reaching movement decomposition on robotic arm control, and also demonstrate the competitiveness of the proposed approach.

A. Chaos Synchronisation Experiments

Accurate capture of targets requires a stable controller, which must be able to converge quickly with a small overshoot. Therefore, a chaos synchronization experiment was designed as shown in Fig. 5 to verify whether the proposed correction movement controller with BENN meet these requirements. In particular, the proposed correction movement controller with BENN was applied to track a chaotic curve, with the results compared with those led by the Sliding Mode Controller (SMC) and single neural network-based Cerebellar Model Articulation Controller (CMAC).

The solid black line in Fig. 5 represents the reference trajectory, generated by a driven system. The yellow, blue and red solid lines represent the trajectories generated by the response systems, which were controlled by the SMC, CMAC and BENN controllers, respectively. The driven system can be represented by the following equation:

$$\ddot{x}_d = -0.3\dot{x}_d + 1.2x_d - x_d^3 + 0.25\sqrt{x_d^2 + \dot{x}_d^2}\sin(0.5t) + 5\cos(0.5t). \tag{21}$$

The response system can be represented as:

$$\begin{aligned}
\ddot{x} = &-0.3\dot{x} + 1.2x - x^3 + 0.25\sqrt{x^2 + \dot{x}^2}\sin(0.5t) \\
&+ 5\cos(0.5t) + \Delta B(x) + l(t) + \tau(t).
\end{aligned} \tag{22}$$

This article has been accepted for publication in a future issue of this journal, but has not been fully edited. Content may change prior to final publication. Citation information: DOI 10.1109/TII.2020.2995142, IEEE Transactions on Industrial Informatics

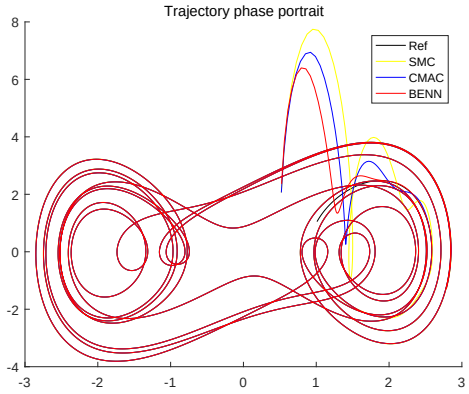

Fig. 5. Trajectory responses of chaos synchronization under SMC (yellow), CMAC controller (blue) and BENN controller (red).

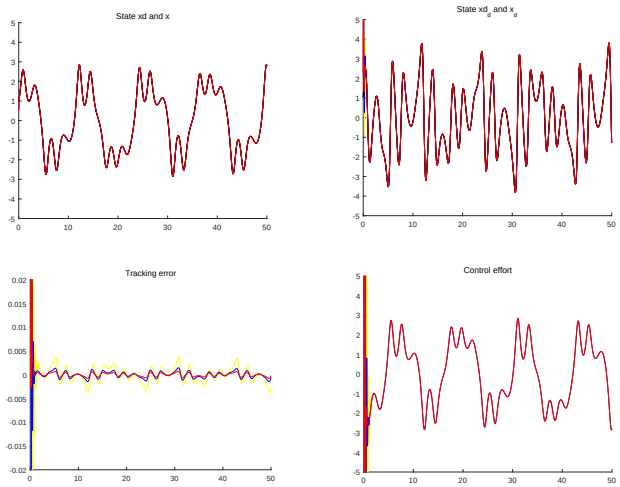

Fig. 6. States x, $\dot{x}$, errors e, and control outputs u of chaos synchronization under SMC (yellow), CMAC controller (blue) and BENN controller (red).

It is clear from the figure that all three trajectories can track chaotic trajectories, but the red trajectory has faster converging speed and less overshoot than the yellow and blue trajectories. This indicates the proposed BENN outperforms the other two reference approaches.

The detailed experimental results are shown in Fig. 6. In particular, Figs. 6(a)-(d) illustrate the tracking response of x, $\dot{x}$, the tracking error e, and the control output τ, respectively. The yellow, blue and red lines represent the control responses from SMC, CMAC, and BENN, respectively. The experimental results show that the proposed BENN has a better control effect and a speedy response, which is important for grasping the target accurately using refined correction movements.

B. Reaching Movement Experiments

Three comparative experiments on reaching movements were designed to demonstrate the control performance of the proposed controller and its sub-comments under the guidance of the vision system:

1) a rough reaching movement driven by the rough reaching movement controller;
2) a smooth correction movement controlled by the correction movement controller;
3) a reaching movement driven by the overall system.

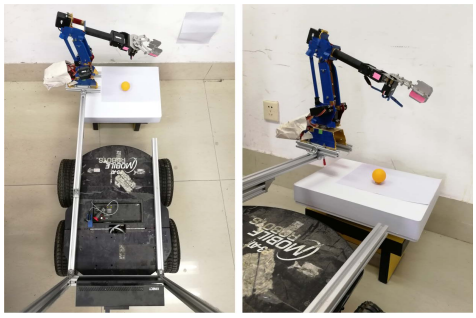

(a) Top view (b) Oblique view

Fig. 7. Top view (a) and oblique view (b) of the experimental environment.

1) Experimental setup: The experimental environment is illustrated in Fig. 7, where the picture in sub-figure (a) was captured from the top view and (b) from the oblique view. The robotic arm was fixed in an initial position. The target was a yellow ball, which was in the operating space of the robotic arm. The experimental goal was that the robotic arm must reach and grasp the ball, and then deliver the ball to a predefined end position, under the guidance of the information captured from the 3-dimensional vision system.

In the three experiments, only four degrees of freedom of the robotic arm were used; i.e., θ_5 is set to 0 based on the task requirement. The posture of the robotic gripper was retained to be vertical downward, thus, $\theta_6 = \frac{\pi}{2} - \theta_2'$. The initial parameter values of BENN were set as: $m = 6$, $n = 12$, $\mu_{ij} \sim [-3.6, 3.6, 0.3]$, $\sigma_{ij} = 1.0$, $\beta = 30$, $\alpha_\eta = 0.01$, $\alpha_{d1} = 1$, $\alpha_{d2} = 10$, $\alpha_W = 0.1$.

2) Experiments using rough reaching movement controller only: A successful reaching movement control with only the rough reaching movement controller is shown in Fig. 8. In particular, sub-figure 8 (1) describes the recognition of the target; 8 (2) shows that the robotic arm was reaching the target; 8 (3) shows the grasping process, and 8 (4) illustrates the robotic arm moving towards the end position. The position coordinates of the target are displayed at the left bottom corner. With only the rough reaching movement applied, the entire reaching movement was completed by one step.

Although the robot with a single neural network controller can have successful reaching, the failure rate of such a controller is high. Due to the inaccuracy of nonlinear mapping and the external disturbances, the robotic arm often bumped into the ball and pushed the ball beyond the workspace. In addition, when a failure occurs, the controller is unable to adjust the arm's gesture based on the error between the current griper's position and the target position, and thus fail the grasping task.

3) Experiments using correction movement controller only: A successful reaching movement generated by the correction movement controller only is demonstrated in Fig. 9. In particular, sub-figure 9 (1) describes the recognition of the target; and 9 (2-12) show the reaching process towards the target. The joint angles of the robotic arm were adjusted step by step based on the position errors between the hand and target, and

This article has been accepted for publication in a future issue of this journal, but has not been fully edited. Content may change prior to final publication. Citation information: DOI 10.1109/TII.2020.2995142, IEEE Transactions on Industrial Informatics

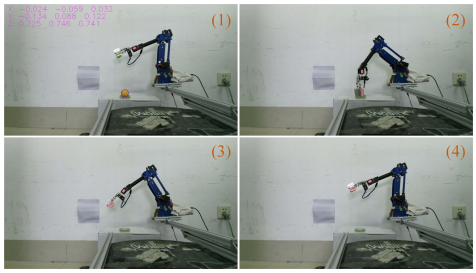

Fig. 8. A successful reaching movement with only rough reaching movement controller.

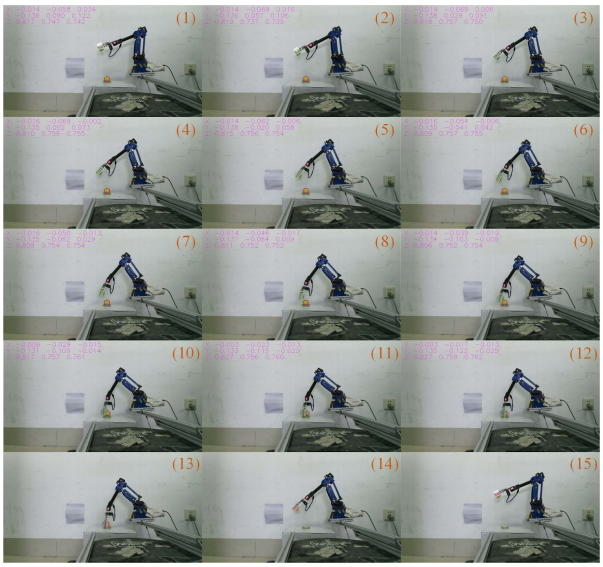

Fig. 9. A successful reaching movement with only correction movement controller.

the whole process took 11 steps. Sub-figures 9 (13-15) show that the robotic arm finally grasped the target and returned to the end position. This experiment only applied the correction movements, and the entire process took 15 steps.

The robotic arm slowly started from the initial position, reached the target and grasped the target, then returned to the end position. Due to the involvement of the visual feedback, the position of gripper was constantly adjusted to reach the target. This control system has a high success rate of grasping. However, if the gripper is too far from the target, the robotic arm must adjust many times, so that it cannot grasp the target quickly.

4) Experiments using dual network-based controllers: This experiment simulated the movement decomposition in human-like reaching movement pattern. Each movement was implemented by either the rough reaching movement controller, or the correction movement controller based on the distance between the grasper and the object, with pre-defined threshold values $D_{\max} = 0.08m$ and $D_{\min} = 0.03m$ in this experiment. If the training of the RBF is unfortunately trapped to a local extreme, its output cannot accurately control the robot arm to reach the target despite not far away. By appropriately adjusting the parameter D_{max}, the robot can still reach a space where the BENN-based controller can be triggered, so as to

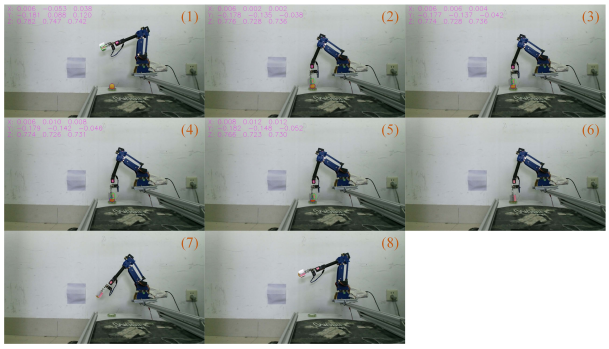

Fig. 10. A successful reaching movement with dual networks-based controller.

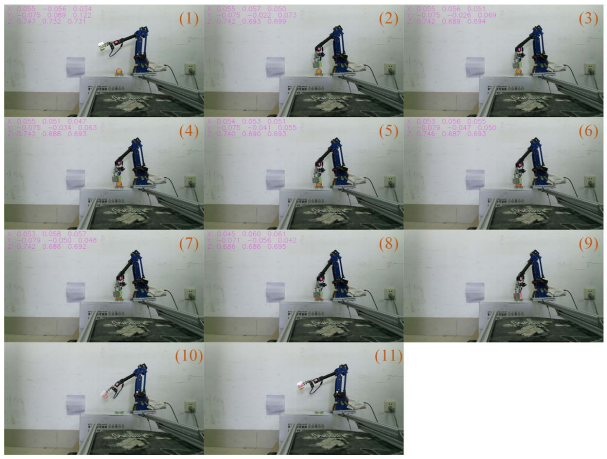

Fig. 11. Another successful reaching movement with dual networks-based controller.

eliminate the effect of the training of RBF controller at the local extreme.

A successful reaching movement process is shown in Fig. 10. Sub-figure 10 (1) shows the image processing module detected the target position. If the system determined that the distance, d, between the gripper and the target was greater than $D_{\max}$, the rough reaching movement controller was called to perform a rough reaching movement as shown in Fig. 10 (2). If $D_{\min} < d < D_{\max}$, the robotic arm applied the correction movement controller to perform a smooth correction movement as demonstrated in sub-figures 10 (3-6). In addition, sub-figures 10 (7-8) show that the robotic arm successfully grasped the target and delivered it to the target position.

Fig. 11 shows another experiment process, with a different target position closer to the robotic arm. The rough reaching movement and the correction movement are shown in sub-figures 11 (2) and 11 (3-8), respectively. In this experiment, the grasper successfully grasped the ball, even though the target was closer to the robotic arm, which made the robotic arm easier to touch the ball and lead to a failure. The same experiments have been repeated many times with different ball and target positions, and the proposed system almost successfully completed all the ball moving tasks, which demonstrated the robustness of the proposed system.

5) Comparison of three control experiments: The three experiments are summarised in Table I based on 30 repetitions

TABLE I
COMPARISON OF EXPERIMENTAL RESULTS.

	num_{all}	num_s	num_f	$rate_s$	avg
pRBF	30	22	8	73.3%	1
BENN	30	28	2	93.3%	13
dual NN	30	29	1	96.7%	6

In this table, pRBF denotes the rough reaching movement controller; BENN denotes the correction movement controller; and dual NN denotes the dual-neural-network based controller.

(i.e., $num_{all} = 30$), with the details of the number of success, num_s, the number of failure, num_f, the success rates, $rate_s$, and the average steps taken, avg. The robotic arm controlled by the rough reaching movement controller only included rough reaching movements, and thus the success rate was the lowest with only 73.3%. The robotic arm controlled by the correction movement controller only had smooth correction movements, and the joint angles were adjusted base on the visual feedback errors detected at each step. Although the success rate was high as 93.3%, the number of adjustment steps was very big, with an average of 13 steps. When the robotic arm was controlled by dual-neural-network controllers in different modes, the success rate reached 96.7%, and the average adjustment step was only 6. This result shows that the proposed system enjoys the advantages of its sub-systems, but compensating the disadvantages of each other; in other words, the proposed robotic hand-eye coordination control system can ensure both real-time response and high success rates.

The experimental results demonstrate the superiority of the proposed system from two perspectives. On one hand, it proves the feasibility of importing human behavior pattern to the robotic grasping arm. Through the movement decomposition, the robotic hand-eye coordination can be completed more effectively. On the other hand, the stability of the control system has been greatly improved by the adaptation of the infant learning patterns, which is consistent with the theoretical proof as presented in Section III-C.

V. CONCLUSION

This paper proposed a new method for robotic reaching movements inspired by the human infant reaching ability development process, and established a visual-guided robotic hand-eye coordination control system. The reaching movement in this work was decomposed and implemented in one of the two neural networks under different conditions. The stability of the control system has been proved by Lyapunov stability theorem. The experimental results showed that the dual neural network-based controller usually leads to higher success rate and better control performance, compared with those control systems with a single neural network. Note that the target ball is supposed to be stationary in this work; therefore, it is interesting to further develop the proposed approach for the tracking and grasping of dynamic targets.

ACKNOWLEDGMENT

The authors are very grateful to the anonymous reviewers for their constructive comments which have helped significantly in revising this work.

REFERENCES

[1] F. Widmaier, D. Kappler, S. Schaal, and J. Bohg, "Robot arm pose estimation by pixel-wise regression of joint angles," in *2016 IEEE International Conference on Robotics and Automation (ICRA)*, May 2016, pp. 616–623.

[2] J. Qu, F. Zhang, Y. Fu, and S. Guo, "Approach movement of redundant manipulator using stereo vision," in *2014 IEEE International Conference on Robotics and Biomimetics (ROBIO 2014)*, Dec 2014, pp. 2489–2494.

[3] B. Jiang, J. Yang, Q. Meng, B. Li, and W. Lu, "A deep evaluator for image retargeting quality by geometrical and contextual interaction," *IEEE Transactions on Cybernetics*, vol. 50, no. 1, pp. 87–99, 2020.

[4] J. Yang, Y. Zhu, B. Jiang, L. Gao, L. Xiao, and Z. Zheng, "Aircraft detection in remote sensing images based on a deep residual network and super-vector coding," *Remote Sensing Letters*, vol. 9, no. 3, pp. 228–236, 2018.

[5] B. Jiang, J. Yang, Z. Lv, and H. Song, "Wearable vision assistance system based on binocular sensors for visually impaired users," *IEEE Internet of Things Journal*, vol. 6, no. 2, pp. 1375–1383, April 2019.

[6] R. Wang, Y. Wei, H. Song, Y. Jiang, Y. Guan, X. Song, and X. Li, "From offline towards real-time verification for robot systems," *IEEE Transactions on Industrial Informatics*, vol. 14, no. 4, pp. 1712–1721, April 2018.

[7] S. Zhang, S. Wang, F. Jing, and M. Tan, "A sensorless hand guiding scheme based on model identification and control for industrial robot," *IEEE Transactions on Industrial Informatics*, vol. 15, no. 9, pp. 5204–5213, Sep. 2019.

[8] P. D. H. Nguyen, T. Fischer, H. J. Chang, U. Pattacini, G. Metta, and Y. Demiris, "Transferring visuomotor learning from simulation to the real world for robotics manipulation tasks," in *2018 IEEE/RSJ International Conference on Intelligent Robots and Systems (IROS)*, Oct 2018, pp. 6667–6674.

[9] A. M. Zanchettin, A. Casalino, L. Piroddi, and P. Rocco, "Prediction of human activity patterns for human-robot collaborative assembly tasks," *IEEE Transactions on Industrial Informatics*, vol. 15, no. 7, pp. 3934–3942, July 2019.

[10] J. Yang, J. Man, M. Xi, X. Gao, W. Lu, and Q. Meng, "Precise measurement of position and attitude based on convolutional neural network and visual correspondence relationship," *IEEE Transactions on Neural Networks and Learning Systems*, pp. 1–12, 2019.

[11] S. Sivcev, M. Rossi, J. Coleman, G. Dooly, E. Omerdic, and D. Toal, "Fully automatic visual servoing control for work-class marine intervention rovs," *Control Engineering Practice*, vol. 74, pp. 153 – 167, 2018.

[12] K. Wu, G. Zhu, L. Wu, W. Gao, S. Song, C. M. Lim, and H. Ren, "Safety-enhanced model-free visual servoing for continuum tubular robots through singularity avoidance in confined environments," *IEEE Access*, vol. 7, pp. 21 539–21 558, 2019.

[13] P. Vicente, L. Jamone, and A. Bernardino, "Robotic hand pose estimation based on stereo vision and gpu-enabled internal graphical simulation," *Journal of Intelligent & Robotic Systems*, vol. 83, no. 3-4, pp. 339–358, 2016.

[14] T. Huynh, C. Lin, T. Le, H. Cho, T. T. Pham, N. Le, and F. Chao, "A new self-organizing fuzzy cerebellar model articulation controller for uncertain nonlinear systems using overlapped gaussian membership functions," *IEEE Transactions on Industrial Electronics*, pp. 1–1, 2019.

[15] F. Chao, Z. Zhu, C. Lin, H. Hu, L. Yang, C. Shang, and C. Zhou, "Enhanced robotic hand-eye coordination inspired from human-like behavioral patterns," *IEEE Transactions on Cognitive and Developmental Systems*, vol. 10, no. 2, pp. 384–396, June 2018.

[16] W. Fang, F. Chao, L. Yang, C.-M. Lin, C. Shang, C. Zhou, and Q. Shen, "A recurrent emotional cmac neural network controller for vision-based mobile robots," *Neurocomputing*, vol. 334, pp. 227–238, 2019.

[17] S. Levine, P. Pastor, A. Krizhevsky, J. Ibarz, and D. Quillen, "Learning hand-eye coordination for robotic grasping with deep learning and large-scale data collection," *The International Journal of Robotics Research*, vol. 37, no. 4-5, pp. 421–436, 2018.

[18] Z. Chen, F. Huang, W. Chen, J. Zhang, W. Sun, J. Chen, J. Gu, and S. Zhu, "RBFNN-based adaptive sliding mode control design for delayed nonlinear multilateral tele-robotic system with cooperative manipulation," *IEEE Transactions on Industrial Informatics*, pp. 1–1, 2019.

[19] F. Chao, D. Zhou, C. Lin, L. Yang, C. Zhou, and C. Shang, "Type-2 fuzzy hybrid controller network for robotic systems," *IEEE Transactions on Cybernetics*, pp. 1–15, 2019.

This article has been accepted for publication in a future issue of this journal, but has not been fully edited. Content may change prior to final publication. Citation information: DOI 10.1109/TII.2020.2995142, IEEE Transactions on Industrial Informatics

[20] M. Antonelli, E. Chinellato, and A. P. Del Pobil, "On-line learning of the visuomotor transformations on a humanoid robot," pp. 853–861, 2013.
[21] W. R. F. Corbetta, D. and S. L. Thurman, *Learning to reach in infancy*. New York: Taylor & Francis, 2018, pp. 18–41.
[22] F. Morange-Majoux, E. Devouche, C. Lemoine-Lardennois, and E. Orriols, "Visual exploration of reaching space during left and right arm movements in 6-month-old infants," *Psychologie Française*, vol. 64, no. 1, pp. 55 – 70, 2019.
[23] D. Corbetta, R. F. Wiener, S. L. Thurman, and E. Mcmahon, "The embodied origins of infant reaching: Implications for the emergence of eye-hand coordination," *Kinesiology Review*, vol. 7, no. 1, pp. 10–17, 2018.
[24] J. Baek, M. Jin, and S. Han, "A new adaptive sliding mode control scheme for application to robot manipulators," *IEEE Transactions on Industrial Electronics*, vol. 63, no. 6, pp. 3628–3637, 2016.
[25] M. Van, S. S. Ge, and H. Ren, "Finite time fault tolerant control for robot manipulators using time delay estimation and continuous nonsingular fast terminal sliding mode control," *IEEE Transactions on Cybernetics*, vol. 47, no. 7, pp. 1681–1693, 2017.
[26] J. Guan, C. Lin, G. Ji, L. Qian, and Y. Zheng, "Robust adaptive tracking control for manipulators based on a tsk fuzzy cerebellar model articulation controller," *IEEE Access*, vol. 6, pp. 1670–1679, 2018.
[27] T.-L. Le, C.-M. Lin, and T.-T. Huynh, "Self-evolving type-2 fuzzy brain emotional learning control design for chaotic systems using pso," *Applied Soft Computing*, vol. 73, pp. 418–433, 2018.
[28] B.-S. Chen, C.-H. Lee, and Y.-C. Chang, "H∞ tracking design of uncertain nonlinear siso systems: adaptive fuzzy approach," *IEEE Transactions on Fuzzy Systems*, vol. 4, no. 1, pp. 32–43, Feb 1996.

Wubing Fang received his BEng. degrees from the China University of Mining and Technology Yinchuan College, in 2013. From 2013 to 2016, he was an Engineer at the Shanxi Xintianyuan Pharmaceutical Chemical Co., Ltd. From 2016, he is working towards his MSc. degree at the School of Informatics, Xiamen University. His research interests include neural network control, robotics, and deep neural networks.

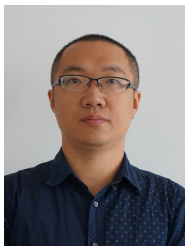

Fei Chao (M'11) received the B.Sc. degree in Mechanical Engineering from the Fuzhou University, China, and the M.Sc. Degree with distinction in Computer Science from the University of Wales, Aberystwyth, U.K., in 2004 and 2005, respectively, and the Ph.D. degree in robotics from the Aberystwyth University, Wales, U.K. in 2009. He is currently an Associate Professor with the School of Informatics, Xiamen University, China. Dr Chao has published more than 50 peer-reviewed journal and conference papers. His research interests include developmental robotics, machine learning, and optimization algorithms.

Chih-Min Lin (M'87-SM'99-F'10) was born in Taiwan, in 1959. He received the B.S. and M.S. degrees from Department of Control Engineering and the Ph.D. degree from Institute of Electronics Engineering, National Chiao Tung University, Hsinchu, Taiwan, in 1981, 1983 and 1986, respectively. He is currently a Chair Professor and the Vice President of Yuan Ze University, Chung-Li, Taiwan. His current research interests include fuzzy neural network, cerebellar model articulation controller, intelligent control systems and signal processing. He also serves as an Associate Editor of IEEE Transactions on Cybernetics and IEEE Transactions on Fuzzy Systems. He is an IEEE Fellow.

Dajun Zhou received his BEng. and MEng. degree from the Cognitive Science Department, School of Informatics, Xiamen University, P. R. China, in 2015 and 2018 respectively. Currently he is a senior software engineer at the Huawei Technologies Co Ltd, China. His research interests include human-robot interactions, machine learning, and intelligent mobile robots.

Longzhi Yang (M'12-SM'17) is currently a Programme Leader and a Reader with Northumbria University, Newcastle upon Tyne, U.K. His research interests include computational intelligence, machine learning, big data, computer vision, intelligent control systems, and the application of such techniques in real-world uncertain environments. He is the Founding Chair of the IEEE Special Interest Group on Big Data for Cyber Security and Privacy. Dr. Yang received the Best Student Paper Award from the 2010 IEEE International Conference on Fuzzy Systems.

Xiang Chang received his BEng. degree in Cognitive Science at the Department of Artificial Intelligence, Xiamen University in 2019. Currently, he is a junior PhD student at the Department of Computer Science, Aberystwyth University. His research interests include deep reinforcement learning based robotic motion planning.

Qiang Shen received the Ph.D. in Computing and Electrical Engineering (1990) from Heriot-Watt University, Edinburgh, U.K., and the D.Sc. in Computational Intelligence (2013) from Aberystwyth University, Aberystwyth, U.K. He holds the Established Chair in Computer Science and is the Pro Vice-Chancellor: Faculty of Business and Physical Sciences, Aberystwyth University. His research interests include computational intelligence and its application in robotics. He has authored two research monographs and over 390 peer-reviewed papers, including one receiving an Outstanding Transactions Paper Award from the IEEE.

Changjing Shang received a Ph.D. in computing and electrical engineering from Heriot-Watt University, UK. She is a University Research Fellow with the Department of Computer Science, Institute of Mathematics, Physics and Computer Science at Aberystwyth University, UK. Prior to joining Aberystwyth, she worked for Heriot-Watt, Loughborough and Glasgow Universities. Her research interests include pattern recognition, data mining and analysis, space robotics, and image modelling and classification.